AIAA SciTech Forum
8–12 January 2018, Kissimmee, Florida
2018 AIAA Information Systems-AIAA Infotech @ Aerospace

10.2514/6.2018-0467

An Iterative Signal Fusion Method for Reconstruction of In-Plane Strain Maps from Strain Measurements by Hybrid Dense Sensor Networks

MK Sadoughi[1], Austin Downey[2], Chao Hu[1,3], Simon Laflamme[2,3]

[1] *Department of Mechanical Engineering, Iowa State University*
Ames, IA 50011 USA

[2] *Department of Civil, Construction, and Environmental Engineering, Iowa State University*
Ames, IA 50011 USA

[3] *Department of Electrical and Computer Engineering, Iowa State University*
Ames, IA 50011 USA

Flexible skin-like membranes have received considerable research interest for the cost-effective monitoring of mesoscale (large-scale) structures. The authors have recently proposed a large-area electronic consisting of a soft elastomeric capacitor (SEC) that transduces a structure's change in geometry (i.e. strain) into a measurable change in capacitance. The SEC sensor measures the summation of the orthogonal strain (i.e. $\varepsilon_x + \varepsilon_y$). It follows that an algorithm is required for the decomposition of the signal into unidirectional strain maps. In this study, a new method enabling such decomposition that leverages a dense sensor network of SECs and resistive strain gauges (RSGs) is proposed. This method, termed iterative signal fusion (ISF), combines the large-area sensing capability of SECs and the high-precision sensing capability of RSGs. The proposed method adaptively fuses the different sources of signal information (i.e. from SECs and RSGs) to build the best fit unidirectional strain maps that can model strain. Each step of the ISF contains an update process for strain maps based on the Kriging model. The proposed method is validated using finite element analysis of a cantilever plate in the Abaqus. The results show that ISF outperforms an existing method in most cases.

I. Introduction

Accurate reconstruction of unidirectional in-plane strain maps over the entire structure of an aircraft is an important tool for local (e.g., localizing material failure) and global (e.g., loss of stiffness) condition assessment. With advances in the field of flexible electronics, the utilization of flexible skin-like membranes has been proposed as a solution for this challenge [1,2]. Additionally, sensing skins that mimic the capability of biological skin to detect and localize damage over a large area have attracted significant attention in the last few years [3]. The authors have previously developed a soft elastomeric capacitor (SEC) designed to be inexpensive with an easily scalable manufacturing process [4]. In contrast with the traditional strain sensors that measure strain at discrete points, SECs measure the additive strain over an area. In situations where the structure's unidirectional strain maps are needed, the main challenge is to decompose the SEC's additive strain map into its linear strain components along two orthogonal directions. To address this challenge, the authors have recently proposed an algorithm that leverages a dense sensor network (DSN) of SECs to decompose the additive strain maps. The algorithm assumes a polynomial deflection shape and appropriate boundary conditions and uses a least squares estimator (LSE) to estimate unidirectional strain maps over the DSN's area. To extend the proposed algorithm, resistive strain gauges (RSG) were added to the DSN to allow for real-time updating of boundary conditions at key locations, therefore, forming a hybrid DSN (HDSN) [5]. This algorithm, termed the extended LSE algorithm, allows for the deployment of HDSNs that combine the mesosurface sensing capability of SECs and mature sensing technology of RSGs capable of precise unidirectional point measurements. This allows HDSNs to act as a sensing skin, capable of monitoring local changes in strain over a global area [6].

Accurate strain map reconstruction necessitates effective fusion of signals from additive and unidirectional strain sensors. The existing reconstruction method uses a least-squares regressor to determine optimum coefficients for deflection shape functions that give the best agreement between the measured and reconstructed strain responses [7]. While computationally efficient, the extended LSE algorithms lacks the ability to reproduce nonlinear strain maps due to its selection of a polynomial deflection shape function. The capability to reproduce nonlinear strain maps is important as damage often manifests itself as nonlinearities in a unidirectional strain map (e.g. a thin crack in a plate). In this study, the authors propose a different approach that overcomes the difficulty of capturing high nonlinearity in strain responses and makes strain map reconstruction suitable for local damage detection. A generic method, termed iterative signal fusion (ISF), is proposed. The method adaptively fuses the different sources of signal information to build an optimum and unique strain map. Each step of the ISF contains an update process for the strain map based on the Kriging model. In the field of surrogate modeling, Kriging or Gaussian process regression is a method of spatial interpolation for which the approximation are modeled by a Gaussian process derived by proper covariances [8,9].

The paper is organized as follow. Section II provides a background on the SEC technology and the use of Kriging to build a surrogate model of a response. Section III introduces the proposed ISF method. Section IV presents the evaluation and validation of the proposed method based on a finite element analysis (FEA) of a cantilever plate.

II. Background

A. Soft Elastomeric Capacitor

The SEC is designed to measure a structure's in-plane (*x*-*y* plane) strain, as shown in Fig. 1. Under the assumption of low sampling frequency (<1000Hz), the SEC can be approximated as a non-lossy capacitor with capacitance *C*:

$$C = e_0 e_r \frac{A}{h} \tag{1}$$

where $e_0 = 8{:}854\,\frac{\mathrm{pF}}{\mathrm{m}}$ and e_r are the vacuum and the polymer relative permittivity, respectively, $A = d \cdot l$ is the sensor area of width d and length l, and h is the thickness of the dielectric. Under the assumption of small strain, the differentiation of Eq. (1) can be written as:

$$\frac{\Delta C}{C} = \left(\frac{\Delta l}{l} + \frac{\Delta d}{d} - \frac{\Delta t}{t} \right) = \varepsilon_x + \varepsilon_y - \varepsilon_z \tag{2}$$

where ε_x, ε_y and ε_z are strains in the x, y and z directions, respectively. Using Hooke's law for in-plane stress, one can rewrite Eq. (2) as follows:

$$\frac{\Delta C}{C} = \frac{1}{1-\nu}(\varepsilon_x + \varepsilon_y) \tag{3}$$

where $\lambda = 1/(1-\upsilon)$ is the gauge factor of the sensor. For SEBS polymers, $\upsilon \approx 0.49$, which results in a gauge factor $\lambda \approx 2$. Based on Eq (3), the signal of the SEC is only a function of the additive strain, $\varepsilon_x + \varepsilon_y$ [10].

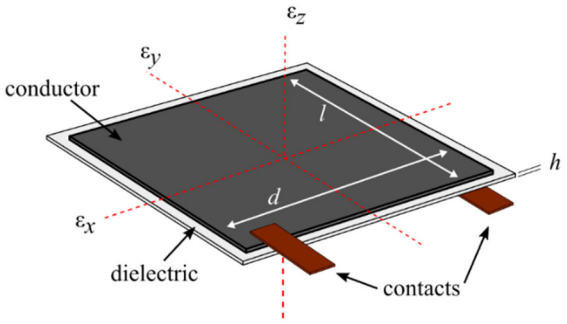

Fig. 1 Schematic of a SEC sensor with reference axes

B. Kriging Model (Gaussian Process)

In Kriging, two main steps are performed simultaneously: (i) build a trend function $\mathbf{h}(\mathbf{x})\boldsymbol{\beta}$; and (ii) build a Gaussian process using the residuals Z [8]. The Kriging-approximated model of the true response $G(\mathbf{x})$ takes the following form

$$\hat{G}(\mathbf{x}) = \mathbf{h}(\mathbf{x})\boldsymbol{\beta} + Z(\mathbf{x}) \tag{4}$$

where $Z(\mathbf{x})$ is a Gaussian process with zero mean, variance s^2, and a correlation matrix Ψ. The elements of matrix Ψ are calculated by the kernel function. The kernel function can take difference form to show the spatial correlation in random space. One popular choice is the squared exponential kernel with a vector of hyper-parameters $\boldsymbol{\theta}$ [11]

$$\psi(\mathbf{x}_i, \mathbf{x}_j) = \exp\left(-\frac{1}{2}(\mathbf{x}_i - \mathbf{x}_j)^T \operatorname{diag}(\boldsymbol{\theta})^{-2} (\mathbf{x}_i - \mathbf{x}_j) \right) \tag{5}$$

where $\operatorname{diag}(\boldsymbol{\theta})$ is a vector with d elements corresponding to d dimensions of $\mathbf{x}$ [12]. The hyper-parameters determines the smoothness of the prediction, and are determined by maximizing the likelihood of observations given $\boldsymbol{\theta}$. Using the Sherman-Morrison-Woodbury formula, the response approximation at a new point $\mathbf{x}$ follows a Gaussian distribution $\hat{G}(\mathbf{x}) \equiv N\left(\hat{G} \middle| \mu_{\hat{G}}, \sigma_{\hat{G}}\right)$ [8]:

$$\mu_{\hat{G}}(\mathbf{x}) = \mathbf{h}(\mathbf{x})\boldsymbol{\beta} + \mathbf{r}(\mathbf{x}) \cdot \Psi^{-1} \cdot (\mathbf{y} - \mathbf{F}\boldsymbol{\beta}) \tag{6}$$

$$\sigma^2_{\hat{G}}(\mathbf{x}) = s^2 \left[1 - \mathbf{r}(\mathbf{x})\Psi^{-1}\mathbf{r}(\mathbf{x})^{\mathrm{T}} + \frac{\left(1 - \mathbf{F}^{\mathrm{T}}\Psi^{-1}\mathbf{r}(\mathbf{x})^{\mathrm{T}}\right)}{\mathbf{F}^{\mathrm{T}}\Psi^{-1}\mathbf{F}} \right] \tag{7}$$

where $\mathbf{h}(\mathbf{x}) = \left[h_1, \ldots, h_p\right]^{\mathrm{T}}$, $\mathbf{y} = [y_1, \ldots, y_t]^{\mathrm{T}}$, and $\boldsymbol{\beta}$ are a vector of p trend functions, a vector of t responses, and a p-element vector of the coefficients of the trend functions, respectively. $r(\mathbf{x}) = [\psi(\mathbf{x}, \mathbf{x}_1), \ldots, \psi(\mathbf{x}, \mathbf{x}_t)]^{\mathrm{T}}$ is a correlation vector between trading and testing points. The process variance s^2 can be determined as $s^2 = \frac{1}{t}(\mathbf{y} - \mathbf{F}\boldsymbol{\beta})^{\mathrm{T}}\Psi^{-1}(\mathbf{y} - \mathbf{F}\boldsymbol{\beta})$. More details about the Kriging model can be found in Ref. [12].

III. Methodology

This work proposes the new ISF method for strain map reconstruction, with an aim to minimize loss of information when fusing signals from hybrid sensors. Suppose the strain measurements made by a hybrid DSN can be grouped into three data sets (see the solid-line boxes in Fig. 2): (i) x-direction strains ε_x at the locations $\mathbf{I}_1$ of x-direction strain sensors, (ii) y-direction strains ε_y at $\mathbf{I}_2$ of y-direction sensors, and (iii) additive strains $\varepsilon_x+\varepsilon_y$ at $\mathbf{I}_3$ of additive strain sensors (SECs). The proposed method iteratively exploits all three strain measurement sets to estimate the strain responses at sensor locations where such responses are not mesured (see the dashed-line boxes in Fig. 2). Each iteration consists of six sequential steps, each of which updates a Kriging (or strain response) model with the most recent strain measurements/estimates and uses the updated model to estimate the strain responses pertaining to one dashed-line box. For example, Step 1 estimates the y-direction strain at $\mathbf{I}_1$ based on all available y-direction strain measurements/estimates, $\mathbf{O}_2^2$ and $\mathbf{O}_2^3$, with the following form:

$$\mathbf{O}_2^1 = GP\left(\mathbf{I}_1 \mid D = \{(\mathbf{I}_2, \mathbf{O}_2^2), (\mathbf{I}_2, \mathbf{O}_2^3)\}\right) \tag{8}$$

where GP is the Kriging-approximated y-direction strain responses at $\mathbf{I}_1$, and $\boldsymbol{D}$ is the y-direction strain data used to update the Kriging model. At Step 2, $\mathbf{O}_2^1$ (i.e. $\hat{\varepsilon}_y$ at $\mathbf{I}_1$) is used to update the additive strain data $\mathbf{O}_3^1$ at the same locations: $\mathbf{O}_3^1 = \mathbf{O}_2^1 + \mathbf{O}_1^1$. After performing the 6 sequential steps, the strain estimates in all dashed-line boxes will be updated. The iteration continues until the amount of changes in the strain values pertaining to all dashed-line boxes converge to zero. As the last step, new Kriging models are built based on all measured/estimated x- and y-direction strain data to reconstruct the unidirectional strain maps, expanded for the entire area of the plate.

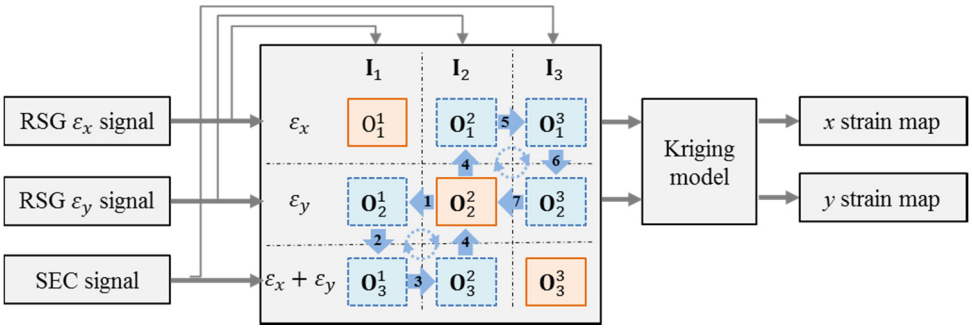

Fig. 2 A flowchart of the proposed ISF method

A pseudo-code of the proposed method is provided in Table 1. A new error estimator, ξ, is defined in line 3 to act as the convergence criterion for the algorithm. If the change of the $\mathbf{O}_2^1$ varies over two sequential iterations converge to the same number (i.e. $\xi < \xi_0$, where $\xi_0 = 0.0001$ in this study), then the algorithm will stop and go to line 11 to build the final model of strain maps.

Table 1 Procedure of ISF using kriging to construct the strain maps

Algorithm 1: Iterative signal fusion

1 Build the initial Kriging model for all three strain maps:
$[\mathbf{O}_1^2, \mathbf{O}_1^3] = \boldsymbol{GP}(\mathbf{I}_2, \mathbf{I}_3 | \boldsymbol{D} = \{\mathbf{I}_1, \mathbf{O}_1^1\})$
$[\mathbf{O}_2^1, \mathbf{O}_2^3] = \boldsymbol{GP}(\mathbf{I}_1, \mathbf{I}_3 | \boldsymbol{D} = \{\mathbf{I}_2, \mathbf{O}_2^2\})$
$[\mathbf{O}_3^1, \mathbf{O}_3^2] = \boldsymbol{GP}(\mathbf{I}_1, \mathbf{I}_2 | \boldsymbol{D} = \{\mathbf{I}_3, \mathbf{O}_3^3\})$
2 **While** $\xi > \xi_0$
3 Calculate the error estimator:
$\xi = \mathbf{O}_2^1 - \boldsymbol{GP}(\mathbf{I}_1 | \boldsymbol{D} = \{(\mathbf{I}_2, \mathbf{O}_2^2), (\mathbf{I}_3, \mathbf{O}_2^3)\})$
4 **Step 1:** *y* strain map at RSG x sensors location:
$\mathbf{O}_2^1 = \boldsymbol{GP}(\mathbf{I}_1 | \boldsymbol{D} = \{(\mathbf{I}_2, \mathbf{O}_2^2), (\mathbf{I}_3, \mathbf{O}_2^3)\})$
5 **Step 2:** Build additive strain map at RSG *x* sensors location:
$\mathbf{O}_3^1 = \mathbf{O}_2^1 + \mathbf{O}_1^1$
6 **Step 3:** Build additive strain map at RSG *y* sensors location:
$\mathbf{O}_3^2 = \boldsymbol{GP}(\mathbf{I}_2 | \boldsymbol{D} = \{(\mathbf{I}_3, \mathbf{O}_3^3), (\mathbf{I}_1, \mathbf{O}_2^1)\})$
7 **Step 4:** Build x strain map at RSG *y* sensors location:
$\mathbf{O}_1^2 = \mathbf{O}_3^2 - \mathbf{O}_2^2$
8 **Step 5:** Build x strain map at SEC sensors location:
$\mathbf{O}_1^3 = (\mathbf{I}_3 | \boldsymbol{D} = \{(\mathbf{I}_1, \mathbf{O}_1^1), (\mathbf{I}_2, \mathbf{O}_1^2)\})$
9 **Step 6:** Build y strain map at SEC sensors location:
$\mathbf{O}_2^3 = \mathbf{O}_3^3 - \mathbf{O}_1^3$
10 **end while**
11 Build the final Kriging models:
$\boldsymbol{\varepsilon_x} = \boldsymbol{GP}((x, y) | \boldsymbol{D} = \{(\mathbf{I}_1, \mathbf{O}_1^1), (\mathbf{I}_2, \mathbf{O}_1^2), (\mathbf{I}_3, \mathbf{O}_1^3)\})$
$\boldsymbol{\varepsilon_y} = \boldsymbol{GP}((x, y) | \boldsymbol{D} = \{(\mathbf{I}_1, \mathbf{O}_2^1), (\mathbf{I}_2, \mathbf{O}_2^2), (\mathbf{I}_3, \mathbf{O}_2^3)\})$

IV. Simulation Study

A. Simulation Setup

Numerical analysis of the proposed method is performed on the model of an aluminum cantilever plate, solved using finite element analysis (FEA) in Abaqus. The model consists of a 1 m x 1 m x 3.175 mm plate, fixed at the left edge as denoted in Fig. 3. The model is constructed using 64,500 plate elements with 9 integration points, a shear modulus of 68.9 GPa was used along with a Poisson's ratio of 0.33, and the density of 2.7 g/cm^3. Two different load

cases are considered. Load case I consists of an upward uniform displacement of 10 cm along the free edge BC as shown in Fig. 3. Load case II represents a cantilever plate where the free edge of the plate is rotated 10 degrees around the bottom left-hand corner of the plate, as shown in Fig. 3.

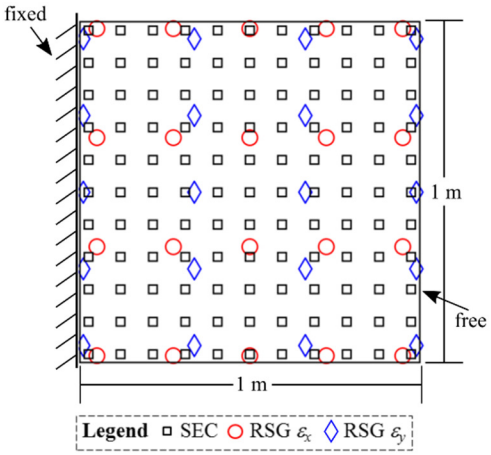

Fig. 3 Sensor locations on the cantilever plate

B. Simulation Results

The ISF-estimated strain maps are reconstructed for the entire area of the plate. The performance of the ISF method is quantified using the mean absolute error (MAE) between the estimated strain maps and the known strain maps (numerical simulations). The number of RSGs at each direction is kept fixed at 20, while the number of SECs is increased from 16 to 400. Fig. 3 shows the locations of sensors based on 121 SECs. Fig. 4 compares the existing LSE method with the ISF method in terms of MAE. The results show that using ISF yields to a lower error in comparison to LSE in most cases. Also, adding SECs yields to constructing more accurate strain maps when the proposed method is used.

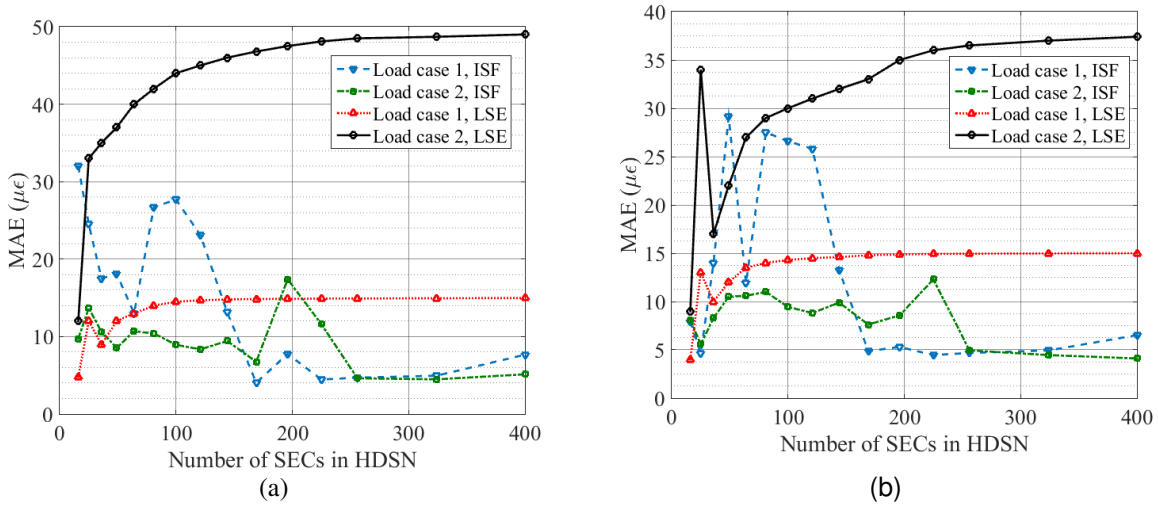

Fig. 4 Comparison between ISF and LSE for two different load cases: (a) MAE error in *x* strain map, (b) MAE error in *y* strain map

Fig. 5 shows the strain reconstruction results for strains ε_x and ε_y in the two principal directions of the cantilever plate under load cases 1 and 2, while the number of SECs are set to 121. As can be seen in this figure, the reconstructed strain maps fit well with the measured data from FEA for both load cases.

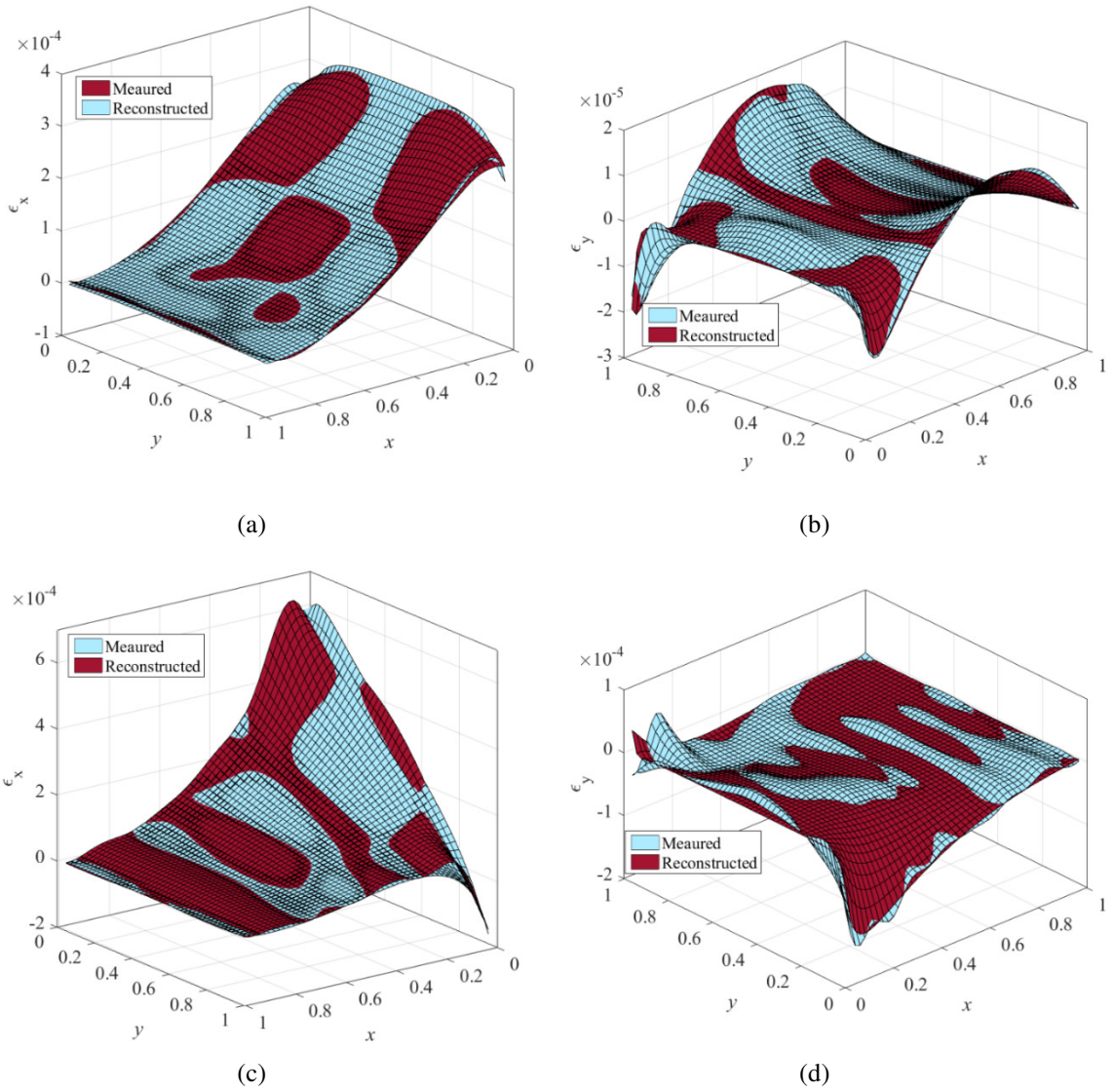

Fig. 5 Reconstructed strain maps in two principal directions for two load cases: (a) *x* strain map for load case 1, (b) *y* strain map for load case 1, (c) *x* strain map for load case 2, and (d) *y* strain map for load case 2.

Acknowledgments

This research was supported in part by the US National Science Foundation (NSF) Grant No. CNS-1566579. Any opinions, findings, or conclusions in this paper are those of the authors and do not necessarily reflect the views of the sponsoring agency.

References

1. Laflamme, Simon, et al. "Dynamic characterization of a soft elastomeric capacitor for structural health monitoring." *Journal of Structural Engineering* 141.8 (2014): 04014186.
2. Rogers, John A., Takao Someya, and Yonggang Huang. "Materials and mechanics for stretchable electronics." *Science* 327.5973 (2010): 1603-1607.
3. Lee, Hyung-Kew, Sun-Il Chang, and Euisik Yoon. "A flexible polymer tactile sensor: Fabrication and modular expandability for large area deployment." *Journal of microelectromechanical systems* 15.6 (2006): 1681-1686.
4. Yoda, Ryuichiro. "Elastomers for biomedical applications." *Journal of Biomaterials Science, Polymer Edition* 9.6 (1998): 561-626.
5. Wu, Jingzhe, et al. "Network of flexible capacitive strain gauges for the reconstruction of surface strain." *Measurement Science and Technology* 26.5 (2015): 055103.
6. Laflamme, Simon, et al. "Damage detection and localization from dense network of strain sensors." *Shock and Vibration* 2016 (2015).
7. Downey, Austin, Simon Laflamme, and Filippo Ubertini. "Reconstruction of in-plane strain maps using hybrid dense sensor network composed of sensing skin." *Measurement Science and Technology* 27.12 (2016): 124016.
8. Rasmussen, Carl Edward. "Gaussian processes for machine learning." (2006).
9. Sadoughi, Mohammad K., Hu, Chao., Mackenzie, Cameron A., Toghi Eshghi, Amin, and Lee, Soobum. "A Maximum Expected Utility Method for Efficient Reliability Analysis of Complex Engineered Systems", Submitted, Structural and Multidisciplinary Optimization, 2017.
10. Saleem, Hussam, et al. "Investigation of dynamic properties of a novel capacitive-based sensing skin for nondestructive testing." *Materials Evaluation* 73.10 (2015): 1384-1391.
11. Bergstra, James, and Yoshua Bengio. "Random search for hyper-parameter optimization." *Journal of Machine Learning Research* 13.Feb (2012): 281-305.
12. Duvenaud, David K., Hannes Nickisch, and Carl E. Rasmussen. "Additive gaussian processes." *Advances in neural information processing systems*. 2011.